Plasma Electrolytic Oxidation (PEO) Layers from Silicate/Phosphate Baths on Ti-6Al-4V for Biomedical Components: Influence of Deposition Conditions and Surface Finishing on Dry Sliding Behaviour

Chiara Bertuccioli [1,3], Andrea Garzoni [2], Carla Martini [2,3,*](ID), Alessandro Morri [2,3](ID) and Gianni Rondelli [4]

1 Imperial College, Tribology Group, SKF University Technology Centre (UTC), 456 City and Guilds Building, South Kensington Campus, London SW7 2AZ, UK; c.bertuccioli18@imperial.ac.uk

2 Industrial Research Centre for Advanced Mechanics and Materials (CIRI-MAM), Alma Mater Studiorum—University of Bologna, Viale Risorgimento 4, 40136 Bologna, Italy; andrea.garzoni2@unibo.it (A.G.); alessandro.morri4@unibo.it (A.M.)

3 Department of Industrial Engineering (DIN), Alma Mater Studiorum—University of Bologna, Viale Risorgimento 4, 40136 Bologna, Italy

4 NanoSurfaces Industries srl, Via Bruno Buozzi 13, 40057 Cadriano di Granarolo nell'Emilia (BO), Italy; rondgia@yahoo.it

* Correspondence: carla.martini@unibo.it

check for updates

Abstract: Plasma Electrolytic Oxidation (PEO) layers were produced on Ti-6Al-4V in different conditions, so as to assess the influence of layer structure, current mode, duty cycle and surface finishing on microstructural features and tribological behaviour. In DC regime, the double-layer structure (silicate bath followed by phosphate bath) beneficially affected wear resistance. In unipolar pulsed DC (phosphate bath), the wear resistance of single layers improved with increasing duty cycle, due to improved microstructure and adhesion: high duty cycle single layers can be considered an alternative to double-layer deposition. Surface finishing by abrasive blasting with spheroidal glass beads leads to surface roughness decrease and hence to decreased friction and improved wear resistance. The best-performing PEO layers showed promising results in the comparison with reference materials such as CoCrMo (both uncoated and (Ti,Nb)N PVD-coated) and PVD-coated Ti-6Al-4V up to 30 N normal load.

Keywords: Plasma Electrolytic Oxidation (PEO); Ti-6Al-4V; friction; wear

1. Introduction

The Ti-6Al-4V alloy is widely used for orthopaedic implants due to its lower elasticity modulus, superior specific strength (strength/density), biocompatibility and enhanced corrosion resistance compared to stainless steels and Co-based alloys. In fact, Chen et al. [1] stated that, among all metallic biomaterials, Ti alloys are the only system which can bond with bone, demonstrating intimate integration with host bone tissue. Conversely, Jarcho et al. [2] observed that bioinert devices such as Co-based implants may induce foreign body responses which contribute to the loosening of permanent implants. Therefore, even though Ti-6Al-4V shows low abrasion resistance and undergoes severe adhesive wear, it provides an important alternative to Co-based alloys: Chen and Thouas [1] demonstrated that Co-based alloys are affected by other limitations due to adverse stress shielding effects as well as to toxic metal ions release. From a metal toxicity point of view, also alloying elements

such as Al and V in Ti-6Al-4V may be associated to long term health problems and newly developed, Al- and V-free alloys were proposed for the biomedical field (e.g., Ti-13Nb-13Zr) [3], however Ti-6Al-4V still covers a large number of applications, considering also non-permanent components such as intramedullary nails and screws.

In order to compensate for possible metal release and, most of all, for the unsatisfactory tribological behaviour of Ti-6Al-4V in implantable biomedical devices, Huang et al. [3] proposed several surface engineering techniques: oxidation produced by either heat treatment or electrolytic anodizing is one of the most popular but also the vapour-phase deposition of carbon-based films (DLC-type) and thermal spraying of hydroxyapatite have been widely investigated. Among oxidation techniques, Plasma Electrolytic Oxidation (PEO), sometimes also named Anodic Spark Deposition (ASD) or Micro-Arc oxidation (MAO), is attracting a significant research and development interest, due to its ability to enhance tribological substrate properties of light alloy and valve metals, forming an effective ion release barrier. Moreover, PEO allows to integrate bioactive components in the growing layer: Durdu et al. [4] demonstrated that it is possible to form hydroxyapatite, calcium apatite-based coatings and to incorporate beneficial ions, such as Ca and P, that enhance the biocompatibility and bioactivity of the surface. Studies by Li et al. [5] on the biological response of Ti implants showed that the PEO process constitutes one of the most successful methods to modify implant surface.

Specifically, Plasma Electrolytic Oxidation (PEO) is based on the modification of the growing anodic layer by spark arc micro-discharges initiated at potentials above its breakdown voltage. This allows the production of thick and adherent coatings mostly consisting of oxides, containing elements from both the metal substrate and the electrolyte solution [6]. The microstructure of PEO coatings is influenced by several factors: (i) type and concentration of electrolyte, (ii) substrate composition and microstructure, (iii) electrical parameters used during the oxidation treatment. PEO electrolytes are commonly alkaline, containing species with pH values typically up to about 13 such as aluminates, phosphates and silicates. PEO layer characteristics are also strongly influenced by polarization conditions such as DC, DC-pulsed (unipolar or bipolar) and AC sources, with control of the current, voltage or power supplied to the cell. The flexibility of electrical regimes allows discharges of intensity suitable to obtain specific microstructures and morphologies. By adjustment of the duty cycle parameters such as pulse duration, frequency and the applied current density, pulsed DC regime allows a better control over the plasma discharge. The pulsed process, reducing the more intense and hence destructive discharge regime, enables the creation of shorter and more energetic micro discharges, leading to more dense coatings. Jiang and Wang [6] found that the use of pulsed DC mode improves homogeneity and reduces the thickness of the porous outer layer (the so-called "technological layer"), resulting in a higher microhardness and a lower coefficient of friction compared to DC regime.

The aim of this work, carried out in a semi-industrial environment, was to optimize the PEO processing conditions for Ti-6Al-4V orthopaedic implants. In particular, PEO layers were produced in different conditions, so as to assess the influence of (i) layer structure (single layer, obtained in phosphate bath or double layer, obtained in silicate bath followed by phosphate bath), (ii) current mode (DC or pulsed DC), (iii) duty cycle (in case of pulsed DC deposition) and (iv) surface finishing (i.e., post-treatment by abrasive blasting) on the tribological behaviour. In fact, Shrestha and Dunn [7] reported that a reduction of PEO surface roughness, in order to remove the typical brittle and porous "technological layer" and to decrease the abrasive contribution to friction in sliding tests, is frequently carried out by conventional laboratory polishing methods. Also, Chen et al. [8] showed that polishing allowed a noticeable decrease of friction coefficient. Fei et al. [9] reported that, for PEO-treated Ti-6Al-4V (silicate-based bath), the coefficient of friction of the polished PEO layer, dry sliding versus SAE52100 steel, was about 50% lower than that of the unpolished one. Wang et al. [10] brought further evidence on the beneficial role of polishing in decreasing friction, both in dry and in solid-lubricated sliding (with graphite top layer). Therefore, in this work, we included an industrial abrasive blasting procedure in the process sequence (after PEO treatment), carried out in typical conditions for implantable metallic components and investigated how abrasive blasting affects the main microstructural features of the

PEO layer, beyond the obvious surface roughness reduction. Hence this paper aims to bring further knowledge also regarding the influence of surface finishing, which plays a very important role in biomedical applications but is seldom the subject of specific investigations.

Hence, this work reports on microstructural and tribological characterization (by dry sliding tests against 100Cr6 (AISI 52100) bearing steel with a block-on-ring contact geometry), aimed to evaluate the influence of the above described process conditions on PEO layer performance. As external references for tribological tests, the following materials were considered: (i) uncoated Co-28Cr-6Mo; (ii) (Ti,Nb)N coated Co-28Cr-6Mo; (iii) (Ti,Nb)N coated Ti-6Al-4V. These references were selected by considering current alternatives for the PEO treatments, based either on the deposition of PVD layers such as (Ti,Nb)N or on the use of a Co-based substrate (uncoated or PVD coated so as to hinder Ni leaching). Thanks to the inclusion of these reference materials in the tribological testing campaign, it was possible to rank the investigated PEO layers among other commercially available solutions: to our knowledge, these data are not available in other papers on this subject.

2. Materials and Methods

2.1. Materials

The substrate for all PEO treatments carried out in this work was the Ti-6Al-4V alloy, supplied by Titanium International Group SrL (Sala Bolognese (BO), Italy) in the form of heat treated extruded bars (solution at 950 °C for 0.5 h, water-quenching, final aging at 515 °C for 8.5 h) with a microhardness of 389 ± 58 HK$_{0.025}$ The surface roughness prior to PEO treatment was 0.20 ± 0.05 μm. The composition of the bars (indicated in the supplier's certificate) was—Al: 5.50–6.75; V: 3.5–4.5; Fe: 0–0.3; H: 0–0.15; N: 0–0.05; O: 0–0.20; C: 0–0.08 (wt.%); Ti to balance.

2.2. PEO Treatment

The main treatment parameters used for the production of the investigated PEO layers are summarised in Table 1.

Table 1. Treatment conditions for the production of PEO layers.

	Layer(s)	Current Mode	Current Density (mA cm^{-2})	Deposition Time (s)	Duty Cycle (%)	Post-Treatment
P	phosphate	DC	30	600	-	abrasive blasting
S	silicate	DC	70	600	-	abrasive blasting
PP	phosphate	Pulsed DC	30	600	60	abrasive blasting
PM	phosphate	Pulsed DC	30	600	72	abrasive blasting
PN	phosphate	Pulsed DC	30	600	80	abrasive blasting
D5	internal: silicate	DC	70	300	-	abrasive blasting
	external: phosphate		70	300	-	
DA	internal: silicate	Pulsed DC	30	600	25	abrasive blasting
	external: phosphate		30	600	68	
DB	internal: silicate	Pulsed DC	30	600	25	none
	external: phosphate		30	600	68	

All the PEO treatments were carried out in galvanostatic regime inside a water-cooled cell (where electrolytes were kept at 5 °C), with Ti-6Al-4V samples as the anode and a grade 1 Ti mesh

as the cathode. Both phosphate-based and silicate-based aqueous solutions were used as electrolytic baths. The silicate-based solution (SiO_2-related compounds 0.015–0.035 mol L^{-1}, pH 11.8) displayed a conductivity of 8.8 mS cm^{-1} at room temperature, whilst the phosphate-based solution (Na_3PO_4 0.05–0.20 mol L^{-1}, pH 12.1) displayed a conductivity of 6.4 mS cm^{-1} at room temperature. For both solutions, KOH was used for achieving the reported pH values.

Three main sets of PEO layers were produced: (i) single layers, DC mode (samples P and S, obtained in phosphate and silicate baths respectively, for preliminary assessment of the influence of abrasive blasting as well as of tribological behaviour); (ii) single layers, unipolar pulsed DC mode, phosphate bath (samples PP, PM, PN, for the evaluation of the influence of duty cycle on coating properties); (iii) double layers (obtained by firstly depositing the internal layer in a silicate bath, then depositing the external layer in a phosphate bath, samples D5, DA and DB).

The layer sequence in double layers was defined on the basis of preliminary tribological testing on PEO single layers obtained in DC mode (samples P and S). A comparison of tribological results from samples P and S (loads to failure in dry sliding, Table 2) indicated that PEO single layers from silicate baths behaved slightly better than those from phosphate baths (in agreement with data summarised by Jiang and Wang [6]).

Table 2. Main features of the investigated PEO layers.

| Title | Layer (s) | Phase Composition, XRD | | | Surface Roughness Ra (μm) | Thickness (μm) | Hardness (HK$_{0.025}$) | Lc3 (N) | Load to Failure in Dry Sliding (N) |
		Anatase (TiO$_2$)	Rutile (TiO$_2$)	Aluminium Phosphate (AlPO$_4$)					
P	single	++	+	-	0.28 ± 0.06	12.8 ± 1.6	380 ± 26	12 ± 3	20
S	single	++	+	-	0.55 ± 0.04	15.2 ± 0.4	410 ± 35	14 ± 2	30
PP	single	++	-	+	0.34 ± 0.06	7.2 ± 0.8	400 ± 169	10 ± 6	30
PM	single	++	-	+	0.48 ± 0.02	6.5 ± 0.9	356 ± 170	15 ± 1	10
PN	single	++	+	+	0.48 ± 0.10	5.1 ± 1.1	390 ± 135	25 ± 1	40
D5	double	++	+	++	0.68 ± 0.04	6.7 ± 1.0	467 ± 71	16 ± 2	40
DA	double	++	+	+	0.65 ± 0.02	5.4 ± 1.9	352 ± 126	21 ± 5	40
DB	double	+	-	+	0.98 ± 0.06	10.9 ± 7.2	290 ± 108	13 ± 1	10

-: not detectable; +: detected; ++: main phase.

Hence, silicate baths were deemed more appropriate for producing the internal layer in double-layered structures. Moreover, the higher surface roughness imparted by the silicate bath (before abrasive blasting, Ra was 3.2 μm for S versus 0.62 μm for P, as shown in Figure 1) was considered advantageous for mechanical interlocking (and hence higher adhesion) of the external layer.

Conversely, samples PP, PM and PN (Table 1) have a single layer structure (obtained by treatment in the same phosphate bath as for P and for the previously mentioned double layers) but for these single layers the PEO treatment was always carried in pulsed DC mode. Phosphate baths were used for single layers due to their ability to produce compact and smooth layers (particularly appreciated for biomedical applications), as well as for their intrinsically higher corrosion resistance and bioactivity, as reported by Jiang and Wang [6]. In the case of single layers from phosphate baths in pulsed DC, the investigations aimed at improving their slightly less advantageous wear resistance by optimising the treatment conditions (namely the duty cycle conditions for the pulsed DC bi-polar square waveform, Table 1).
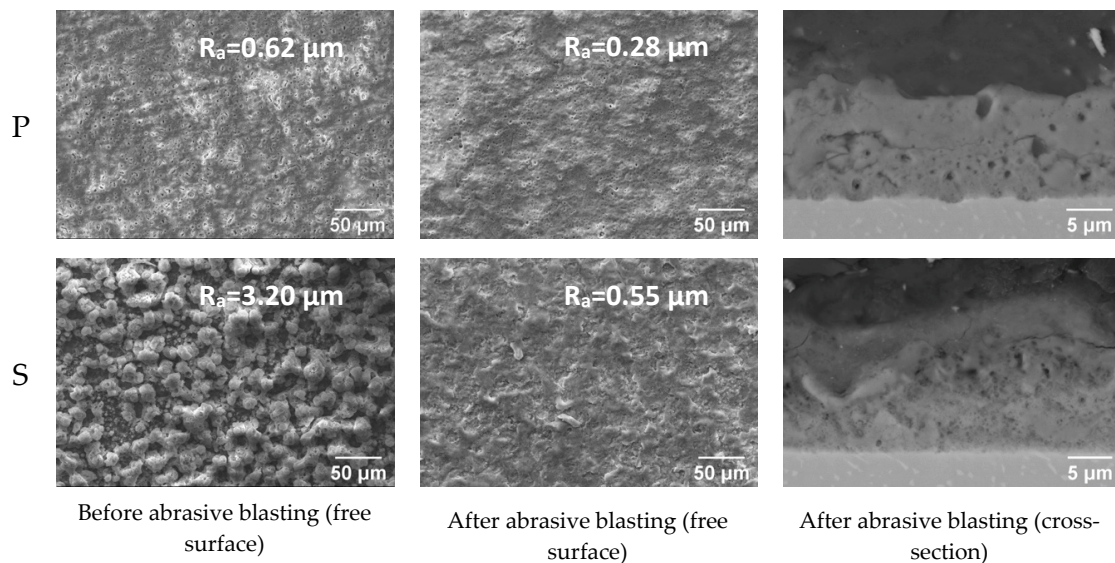
| | Before abrasive blasting (free surface) | After abrasive blasting (free surface) | After abrasive blasting (cross-section) |

Figure 1. Free surface morphology of PEO single layers obtained in phosphate (P) or silicate (S) bath (DC mode), before (left) and after (centre) abrasive blasting (SE images). Cross-sections of the same layers after abrasive blasting (right, BSE images).

The abrasive blasting post-treatment mentioned in Table 1 was carried out by using spheroidal glass beads (100 ± 10 μm average diameter, average elemental composition measured by EDS, wt.%: Si 30, O 52, Na 9, Ca 6, Mg 2, Al 1) as abrasive medium in an industrial blasting device used for implantable metallic components. In fact, a low surface roughness is required in tribological contacts, so as to limit the production of hard wear debris which also adversely affect the biological response [3]. Therefore, all the PEO-treated specimens were abrasive-blasted, with the exception of sample B, used only as a reference: by comparing it to sample A, obtained in the same treatment conditions, it is possible to assess the influence of the abrasive blasting process on microstructure and tribological behaviour of PEO layers.

2.3. Microstructural and Micro-Mechanical Characterization

Surface and cross-sectional analyses of the microstructure of the PEO-treated specimens were performed by means of a scanning electron microscope (SEM, Zeiss EVO 50, Oberkochen, Germany) in low vacuum mode.

X-ray diffraction (XRD, Panalitycal, Eindhoven, Netherlands was used for assessing the phase composition of PEO layers. Analyses were carried out by performing θ–2θ scans from 20° to 90° with a 0.05 step size and a 5 s dwell time, by a Philips PW1729 X-ray diffractometer with a Cu-Kα radiation source (λ = 0.15406 nm, Ni-filter), at 40 kV and 30 mA. XRD patterns were collected from the free surface of PEO layers.

A Renishaw InVia micro-spectrometer (Renishaw plc, New Mils, UK), coupled with a Leica DMLM microscope, using the 50 mW Ar$^+$ laser (wavelength: 514.5 nm) as excitation source, was used to acquire Raman spectra. The analyses were performed by focusing the laser on spots of about 2 μm diameter and, in order to avoid sample degradation, different filters were used to reduce laser power.

Glow Discharge-Optical Emission Spectroscopy (GD-OES, Spectruma Analitik GDA 650, Hof, Germany) concentration versus depth profiles were carried out on PEO-treated specimens. Before each analysis surface contamination was removed by ethanol rinsing. The profiles were obtained with a Grimm-style glow discharge lamp in RF mode. The analysed area in each measurement was about 5 mm^2, corresponding to the internal area of the tubular anode (2.5 mm diameter). A rotary pump was used to evacuate the Grimm-type atomisation/excitation source down to a pressure of 0.05 hPa.

Argon was used as working gas (99.995% purity) and after evacuation it was injected to a constant pressure of 3 hPa.

Surface roughness measurements were carried out on coating free surfaces by stylus profilometry (Hommelwerke T2000, stylus tip: 5 µm curvature radius, Villingen- Schwenningen, Germany). Microhardness was evaluated on the free surface of PEO-treated samples by means of Knoop ($HK_{0.025}$) indentation testing.

The practical adhesion of the anodic oxides was assessed by means of scratch tests, according to the International Standard ISO 20502 [11], using a Revetest XPress device (Anton Paar GmbH, Graz, Austria) with a Rockwell diamond indenter (200 µm spherical tip radius). Scratch tests were carried out by applying a linearly increasing load (from 1 to 30 N), with a 10 mm scratch length and a 10 mm/min speed rate.

2.4. Dry Sliding Tests

A flat-on-cylinder tribometer (block-on-ring contact geometry, ASTM Standard G77 [12], described in further detail elsewhere by Ceschini et al. [13], was used to carry out dry sliding test on both untreated Ti-6Al-4V and PEO-treated samples. Stationary blocks consisted of the PEO treated specimens (as well as of the untreated alloy and of the reference materials for comparison described in Section 2.5), whilst the counter material was a 100Cr6 (AISI 52100) bearing steel cylinder (60 HRC, Ra = 0.2 µm). Sliding tests were performed at room temperature (between 20 and 23 °C) with a relative humidity ranging from 50% to 60%. The sliding speed was fixed at 0.3 m s^{-1}, while the sliding distance was set at 1000 m. The normal load was maintained constant in each test, ranging from 5 to 40 N. This led to initial maximum Hertzian contact pressures from 40 to 100 MPa on PEO layers (considering anatase as prevalent phase for the treated specimens, as indicated by phase identification results obtained in this work and deriving anatase mechanical properties from literature values of Borgese et al. [14] and Soares et al. [15]. A bending load cell was employed for continuously recording friction force as a function of sliding distance. The coefficient of friction (COF) was evaluated for each test by averaging steady-state data. The COF value for each condition and each sample was then calculated by averaging the COF of at least 3 test repetitions. The same stylus profilometer described in Section 2.3 was used to evaluate both wear scar depths and widths on both flat blocks and rotating cylinders. Wear depth values were determined by averaging at least 3 profiles on each wear scar and then averaging again the mean values over the repetitions. The dominant wear mechanisms were identified by carrying out analyses of the worn surfaces and wear debris by means of a Hirox KH 7700 3D-digital microscope (Hirox Co Ltd., Tokyo, Japan) as well as by SEM-EDS (SEM, Zeiss EVO 50, Oberkochen, Germany).

2.5. References for the Comparison of Tribological Behaviour

The tribological behaviour of PEO-treated Ti-6Al-4V was compared with the following references: (i) uncoated Co-28Cr-6Mo; (ii) (Ti,Nb)N coated Co-28Cr-6Mo; (iii) (Ti,Nb)N coated Ti-6Al-4V.

The PVD (Ti,Nb)N coating was considered as reference for comparison because Galetz et al. [16] and Malchesky [17] showed that it produced a low friction coefficient against polyethylene. Moreover, Paschoal et al. [18] proved that (Ti,Nb)N is an effective barrier against ion release from the substrate. The PVD (Ti,Nb)N coating was deposited on both substrates by an industrial Arc Evaporation process. The main features of the PVD coating were—thickness 5.0 µm, hardness 2300 $HV_{0.01}$, surface roughness 0.26 ± 0.05 µm.

The Co-28Cr-6Mo alloy (ASTM F1537 [19], Low-Carbon type) was in the wrought, un-annealed state (42 HRC, grain size 10 according to ASTM E112 [20], surface roughness 0.20 ± 0.11 µm).

3. Results and Discussion

3.1. Phase Composition (General Remarks)

The main features of the PEO layers are summarized in Table 2. In several layers, the main phases detected by XRD (which analyses the coating full-thickness composition, as demonstrated by the presence of peaks from the substrate) are the two crystalline forms of TiO_2: anatase and rutile (Table 2). Representative XRD spectra, recorded on single layers from silicate- or phosphate-rich baths (samples S and P, respectively) are reported in Figure 2.
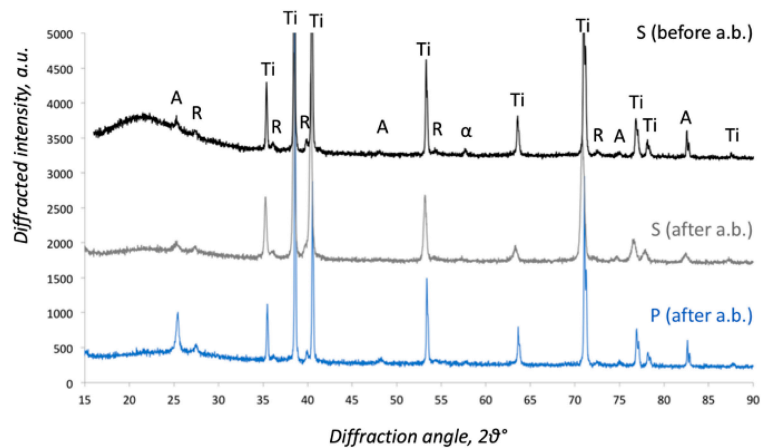
Figure 2. Indexed XRD patterns (Cu Kα radiation) characteristic of the through-thickness composition of PEO single layers obtained in DC mode from silicate- or phosphate-based baths (a.b.: abrasive blasting). Ti: Ti-6Al-4V; A: anatase (TiO_2); R: rutile; α: α-Al_2O_3

XRD patterns for sample S in Figure 2 also show the influence of abrasive blasting on phase composition but this point will be discussed subsequently (Section 3.2).

Anatase was the dominating phase in XRD patterns of all samples (Table 2) and it was the only phase detected by micro-Raman (Figure 3), using spectra reported in Bouchard and Smith [21] as references for Raman peaks indexing. Further reference spectra were found in Friedemann et al. [22].
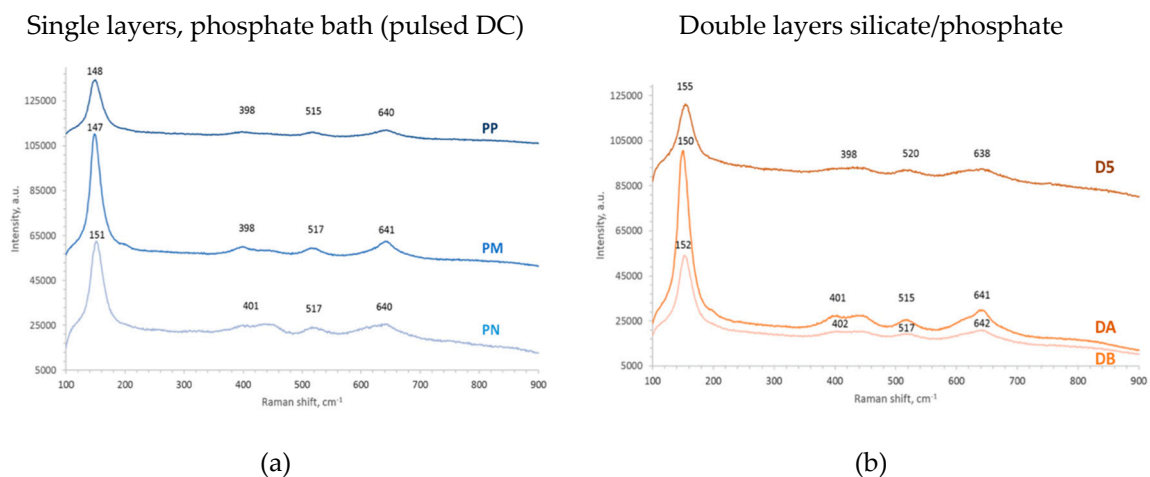

Figure 3. Raman spectra (λ = 514.5 nm) on free surfaces of PEO single (**a**) and double layers (**b**). All indexed peaks are assigned to anatase.

The inability of Raman (characterized by a shallower penetration through the PEO layer than XRD) to detect rutile may be due to the higher concentration of the anatase in the outermost portion of

the PEO layers. In fact, prevalence of the metastable oxide in the outer portion of PEO layer, where a high cooling rate and hence rapid quenching is likely to predominate on annealing effects, has been observed also in the case of aluminium alloys by Xue et al. [23].

The prevalence of anatase over rutile both in single layers (P, PN) and in double layers (DA) obtained in pulsed DC is most likely due to the use of phosphate-based baths (either for the single layer or for the external layer in double-layered architectures). In fact Khan [24] showed that phosphate baths in DC mode are known to produce anatase-rich PEO layers, where phosphorus, incorporated during the growth, tends to limit the anatase to rutile transformation (which is the final transformation in the sequence from amorphous titania to metastable anatase (T > 550 °C) and then to thermodynamically stable rutile (T > 850 °C) under the action of micro-arc discharges.

By comparing samples DA and DB (treated in the same conditions and differing only in the abrasive blasting post-treatment carried out on DA, Table 1), it is possible to notice that a minor contribution of rutile was detectable by XRD only in the abrasive-blasted sample DA, probably due to the smoother surface that improves the signal-to-noise ratio.

In all the layers produced by phosphate-based electrolyte (with the exception of the DC mode single layer P), also some orthorhombic aluminium phosphate ($AlPO_4$) was detected (Table 2), as observed by Martini et al. [25] in a previous work on PEO treatment of Ti-6Al-4V. According to Wang et al. [26], crystalline $AlPO_4$ is supposed to form as a consequence of high-temperature thermolysis of hydrated aluminium polyphosphates inside discharge channels. In single layers S and P (DC mode), also traces of α-Al_2O_3 were detected by XRD (Figure 2), as previously observed by Yerokhin [27] for PEO treatment of Ti-6Al-4V. In this work, silicate-based electrolyte in DC (sample S) did not produce a rutile-dominated layer, as the one observed by Yerokhin as well as by Wang [27,28] in AC-treated Ti-6Al-4V (phosphate-based bath). In our case, the prevalence of anatase may be due to less intensive arcing and lower temperatures inside discharge channels.

As regards the influence of the incorporation of P-based compounds in the PEO layers on biological response (which has not been investigated yet for these layers), literature data indicate that P-containing PEO coatings on Ti-6Al-4V induce a homogeneous distribution of growing MG-63s cells as well as a higher collagen deposition per cell than plasma-sprayed hydroxyapatite [29]. Also, the incorporation of Si (as amorphous silicate) is not expected to have a negative impact on biological response (SiO_2-based bioactive materials are known for their excellent bioactivity [30]). However, the actual biological response to these PEO layer will require specific investigations in a further step of the work.

The influence of treatment conditions and surface finishing on microstructure, phase composition and micro-mechanical properties will be discussed in the following Sections 3.2–3.4). Subsequently, the tribological behaviour of all the PEO layers will be discussed and compared to selected reference materials in the final Section 3.5.

3.2. Influence of Abrasive Blasting

The influence of abrasive blasting on surface morphology and roughness is shown in Figure 1 for PEO single layers obtained in DC mode (P and S in Table 1).

The comparison of images and Ra values in Figure 1, before and after abrasive blasting, shows that this mechanical surface finishing treatment effectively removes the brittle and porous external layer of the anodic oxides, most notably in the case of samples from silicate-based baths (S). For the S samples, the free surface displays a rough appearance, with nodular features (ranging from about 5 to 20 μm) and large pores between the nodules, typical of PEO layers grown in silicate-rich electrolyte as shown by Aliasghari et al. [31]. In the case of samples treated in the phosphate-based solution (P), which already showed a rather smooth surface morphology in the as-treated condition, the decrease of surface roughness as well as the morphological modification is less remarkable. In fact, also after abrasive blasting, typical PEO defects due to stochastic discharge events and gas evolution, such as cavities and volcano-like features, are still visible in P samples.

For samples obtained in silicate baths (S), the influence of abrasive blasting on phase composition is shown in Figure 2, where XRD patterns recorded before and after mechanical surface finishing are compared. In this case, the most evident effect of abrasive blasting is the removal of the amorphous contribution (wide band at low diffraction angle), likely due to amorphous silica as suggested by Wang et al. [28]. Also, Yerokhin et al. [27] detected amorphous silica in PEO layers produced on Ti-6Al-4V in silicate-based baths. In fact, also large-area EDS analysis (Table 3) displays a remarkable decrease in Si concentration after blasting (from about 28 to 15 wt.%).

Table 3. Surface composition of the PEO layers (EDS, wt.%; average data, recorded on several areas imaged at 500× on each sample) before and after abrasive blasting (a.b.).

Title	Title	O	Ti	Al	V	Na	K	Si	P
P	Before a.b.	48.3 ± 0.9	40.1 ± 0.1	2.4 ± 0.1	0.8 ± 0.2	0.4 ± 0.1	-	0.2 ± 0.1	7.8 ± 0.1
	After a.b.	47.8 ± 0.8	39.5 ± 0.5	2.5 ± 0.1	1.3 ± 0.1	0.5 ± 0.1	-	0.4 ± 0.1	8.0 ± 0.1
S	Before a.b.	58.3 ± 0.4	8.4 ± 0.3	0.3 ± 0.1	0.4 ± 0.1	0.7 ± 0.1	0.6 ± 0.1	27.9 ± 0.7	3.4 ± 0.1
	After a.b.	56.6 ± 0.6	22.9 ± 0.4	1.4 ± 0.1	0.9 ± 0.1	0.5 ± 0.1	0.3 ± 0.1	15.0 ± 0.1	2.4 ± 0.1

The influence of abrasive blasting on surface composition was also evaluated for single layers deposited from phosphate baths in pulsed DC mode (PP, PM, PN, Table 1), in order to check for accumulation of Si from the blasting medium also in this set of samples. Results of large-area EDS analysis on the free surface demonstrated that sample PP (obtained at lowest duty cycle, that is, at lowest pulse-on times) shows a significantly higher Si concentration (visible also in cross-section X-ray maps discussed in Figure 4) than the others.

The shorter pulse-on times for the treatment of sample PP may be responsible for a lower density of the layer, as shown by cross-sections in Figure 4, hence for the increased tendency to abrasive incorporation by comparison to other PEO layers obtained in pulsed DC. In this current regime, also Dehnavi et al. [32] observed that layer density and microstructure improved with increasing pulse-on time. This Si enrichment is likely to be responsible for the relatively high microhardness of sample PP (Table 2), thus beneficially influencing its tribological behaviour.

These results show that, also for the S single layers discussed above (Table 3), surface contamination due to Si from the blasting medium cannot be ruled out, because it can be masked by the decrease of Si% as a consequence of the removal of the outermost amorphous silica layer. Therefore, in the case of silicate-phosphate double layers (DA and DB, Table 1), the possible surface enrichment of Si due to abrasive blasting was assessed by measuring GD-OES depth profiles (Figure 5), in order to take into appropriate consideration also the layered structure of the coatings.

Glow Discharge-Optical Emission Spectroscopy (GD-OES) depth profiles in Figure 5 show the trend of Ti, Si and P signal intensity as a function of depth for the same double layer coating, both before (as-treated) and after abrasive-blasting. Oxygen was not included in this graph because its profile typically has a lower S/N ratio than the others and it would affect readability without yielding further useful information. Also, Al and V, which showed similar trends as Ti but with proportionally lower intensity due to their lower alloy concentration, were not added in the graph so as to preserve its readability. Based on the comparison of Si profiles, abrasive blasting decreases the total layer thickness of about 10 μm (from 15 to 5 μm). Such an estimate is probably more accurate than the one obtainable by polished cross-sections (Table 2), because GD-OES data are averaged over a relatively large analysed area whilst the intrinsic brittleness of as-treated PEO layers makes them prone to damage during metallographic preparation.
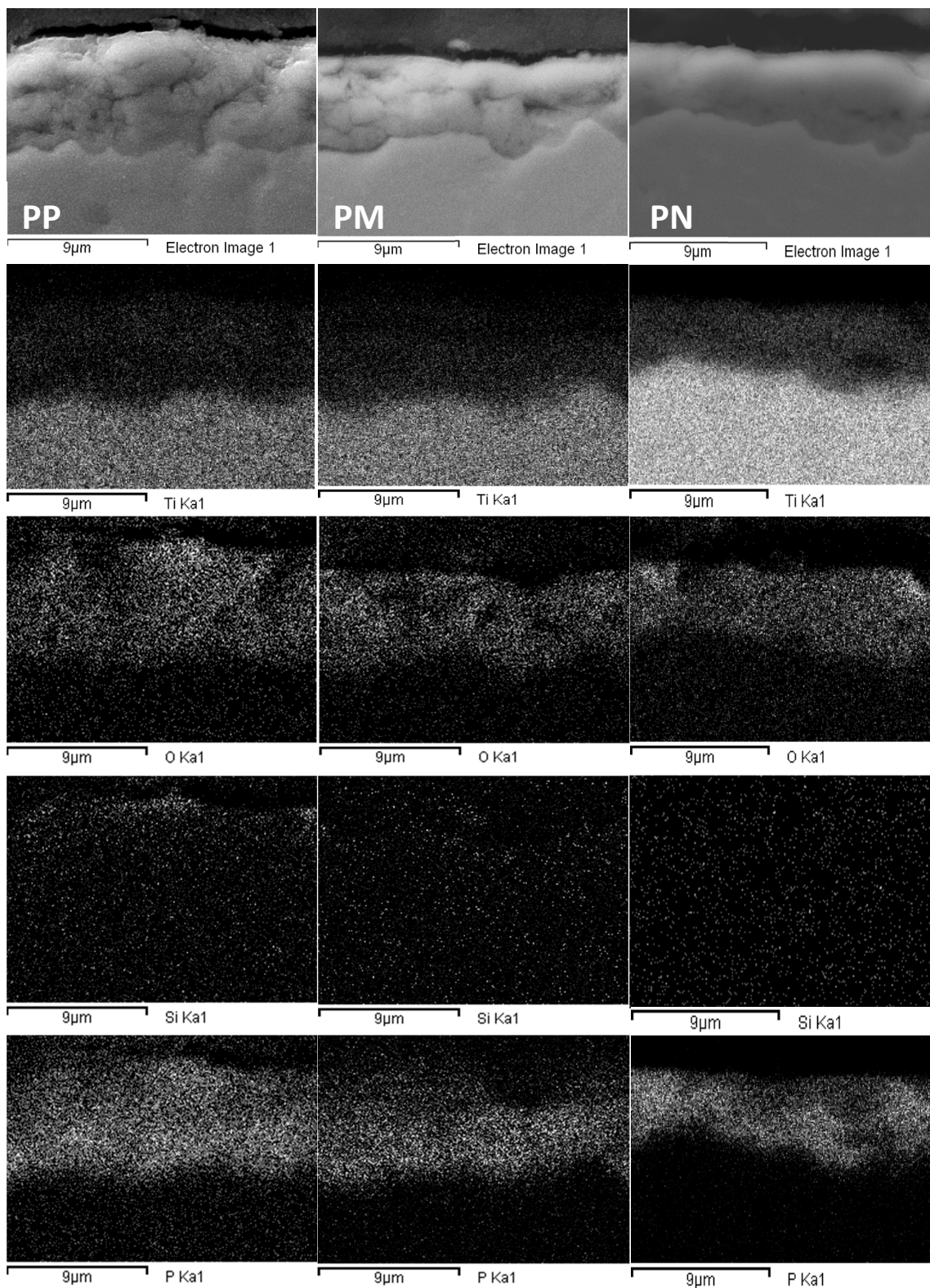
Figure 4. Polished cross sections and EDS X-ray maps of single layer PEO coatings obtained in pulsed DC (phosphate bath): PP (left column), PM (centre column) and PN (right column). The duty cycle increases on going from left to right (Table 1). The X-ray maps were recorded for each coating in the same area of the electron image in the top row.
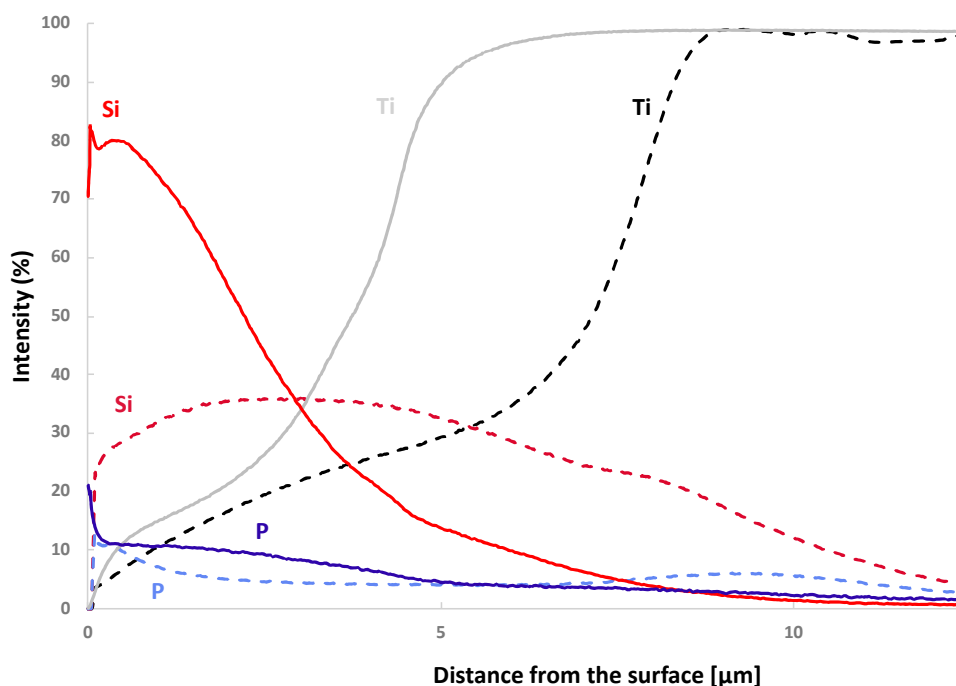
Figure 5. GD-OES depth profiles of Si, Ti and P measured from the free surface of PEO double layers DA (abrasive-blasted, solid lines) and DB (as-treated, dashed lines) obtained by treatment in silicate bath followed by phosphate bath.

In the as-treated double layer (DB), P can be detected through the whole thickness of the PEO layer and its signal shows a slight intensity increase at around 10 μm from the surface. In the abrasive-blasted layer (DA), thinned and compacted by the finishing procedure, the P signal is more intense than in the previous case and rather constant throughout the layer thickness, indicating in both cases that the electrolyte was able to penetrate the inner regions of the coating, probably through breakdown channels, as observed also by Galvis et al. [33] for single layers obtained in DC mode from phosphate baths. Even though the immersion in the phosphate solution was the second step of the treatment, after the first step in silicate bath, it induced P enrichment of the whole layer (as shown also by EDS X-ray maps in Figure 4). GD-OES depth profiles also show a remarkable increase of Si in the outermost portion of the abrasive-blasted layer (DA), by comparison to the same coating in the as-treated condition (DB). The different trend and the higher concentration of Si in the abrasive-blasted layer (DA) is most likely due to embedding of silicate glass fragments during abrasive blasting.

3.3. Influence of Current Mode (DC Versus Pulsed DC)

In the case of phosphate-based single layers, the influence of current mode can be estimated by comparing sample P (DC mode) with PP, PM, PN (pulsed DC). Cross-section images in Figure 1 (sample P) and 4 (PP, PM, PN), as well as average thickness values in Table 2, show that the use of pulsed DC current induces a slight densification of the PEO layer, accompanied by a thickness decrease. This is probably due to the beneficial influence of pulse-off time which, in the pulsed DC mode, contribute to interrupt spark discharges, decreasing the growth rate but also limiting disruptive discharge events. In terms of phase composition, the use of pulsed DC slightly reduced the tendency towards the formation of stable rutile (Table 2), probably due to the attainment of lower temperatures than in DC mode. In terms of micromechanical properties (Table 2), there is no remarkable difference between microhardness and critical loads for full delamination (Lc3) among samples obtained in DC or pulsed DC mode. However, the PN layer, obtained in pulsed DC at the highest duty cycle

(Table 1), makes an exception, with its highest Lc3 value due to improved microstructure (discussed in Section 3.4).

In the case of double layers, the influence of current mode on microstructure can be assessed by comparing sample D5 (DC mode) with DA (pulsed DC). The cross-section images in Figure 6 show that both samples do not display significant porosity.
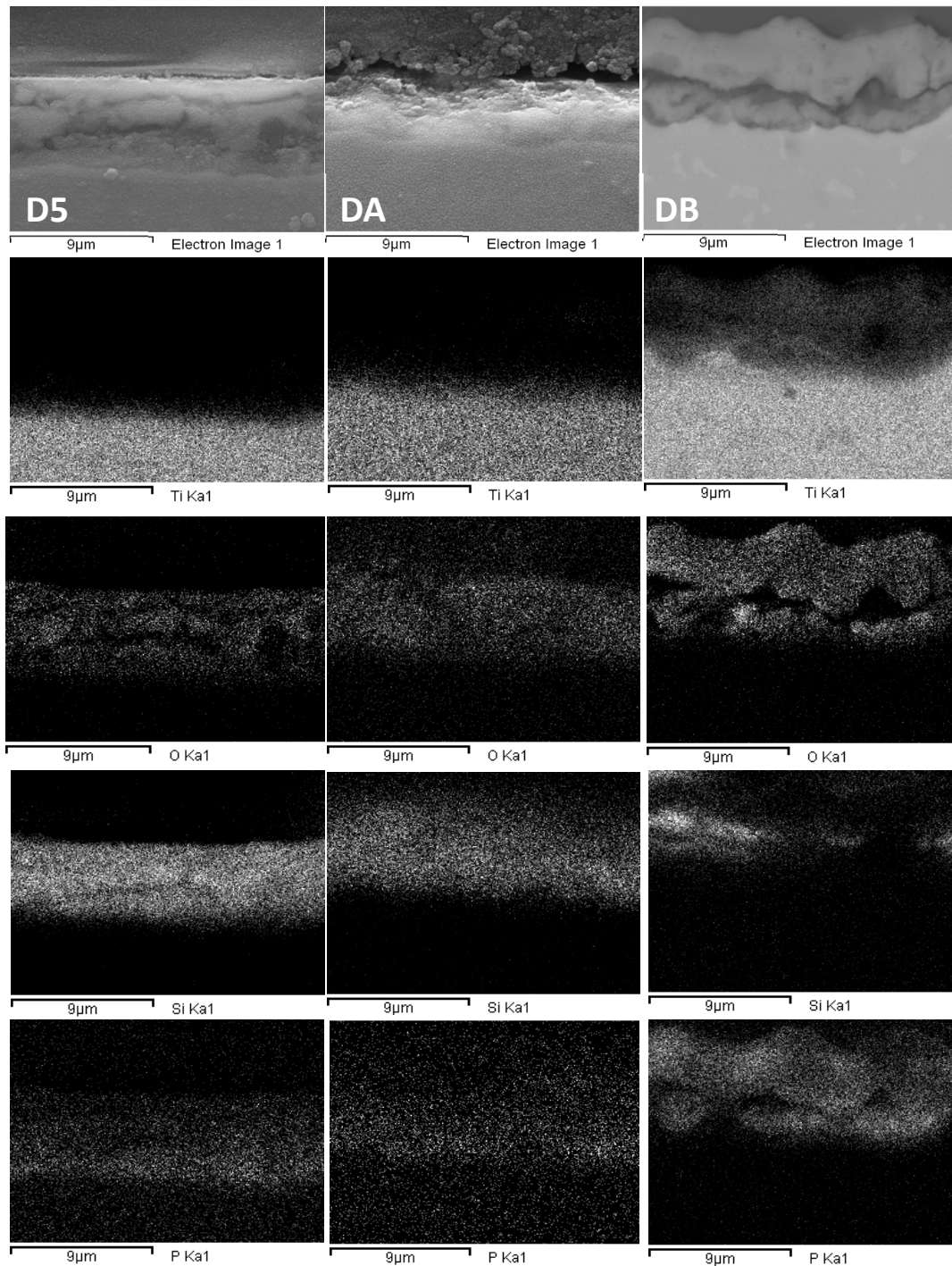

Figure 6. Polished cross sections and EDS X-ray maps of double layer PEO coatings (silicate bath followed by phosphate bath): D5 (top column), DA (centre column) and DB (right column). More information on deposition conditions of double layers can be found in Table 1. The X-ray maps were recorded for each coating in the same area of the electron image in the top row.

Double-layered sample DA is slightly thinner and less compact that D5, mostly in the outer zone. The only difference in terms of phase composition between these samples was a higher amount of crystalline AlPO$_4$ in the layer obtained in DC mode (D5), where high-temperature thermolysis of hydrated aluminium polyphosphates inside discharge channels was probably more likely than in pulsed DC (where pulse-off time may allow cooling during coating growth in a more effective way). In pulsed DC mode (sample DA), a lower current density was employed (Table 1), further contributing to the achievement of lower temperatures during discharge events. The use of pulsed DC lead to lower thickness and microhardness in sample DA but it induced a higher practical adhesion (Lc3) by comparison to D5 (Table 2).

3.4. Influence of Duty Cycle (Pulsed DC)

For phosphate-based single layers in pulsed DC (PP, PM and PN, Table 1), thickness decreased whilst compactness increased with increasing duty cycle (Figure 4), due to the beneficial microstructural effect of increasing pulse-on time, as previously discussed in Section 3.2. Accordingly, in terms of phase composition, rutile was detected only at the highest duty cycle values, in sample PN (Table 2). Correspondingly, a relatively high microhardness was detected in the same sample. The highest microhardness recorded for phosphate-based single layers was recorded in sample PP, obtained at the lowest duty cycle value: however, in this case the measured value in probably affected by the abrasive residues embedded in the surface layer, as previously discussed in Section 3.2.

In general, the low hardness of these PEO layers, which are only slightly higher than the substrate, may be due to the predominance of soft anatase (Table 2), as well as to residual non-oxidised titanium, as suggested also by Yerokhin et al. [27]. Also, Diamanti et al. [34] obtained a similar result, that is, thin anatase-based PEO layers on Ti-6Al-4V, produced in calcium glycerophosphate bath, displayed a hardness lower than the untreated substrate.

The microstructural modifications induced by the increase of duty cycle also showed a beneficial influence on practical adhesion (Lc3, Table 2), which can be ascribed to the denser microstructure [35,36].

3.5. Dry Sliding Tests

Average values of coefficient of friction (COF) as well as of maximum wear depth are plotted as a function of normal load in Figure 7.

Each PEO layer is characterised by a critical normal load (Table 2) at which failure of the coating occurs during the test, hence the load range for COF values in Figure 7a is wider for the best-performing coatings than for the worst ones.

Figure 8 shows the typical graph recorded during the tests which induced coating failure: when the substrate starts to be involved in the contact (after about 100 m in this case), COF decreases whilst system wear (i.e., material removal from both the block and the ring) increases with increasing sliding distance. The friction transition after coating failure lead to COF values comparable to that of the untreated substrate.

The observation of wear scar morphology after the above described friction and wear transitions (Figure 9) shows that, after coating failure, the underlying substrate is deeply ploughed (Figure 9b) due to abrasion.
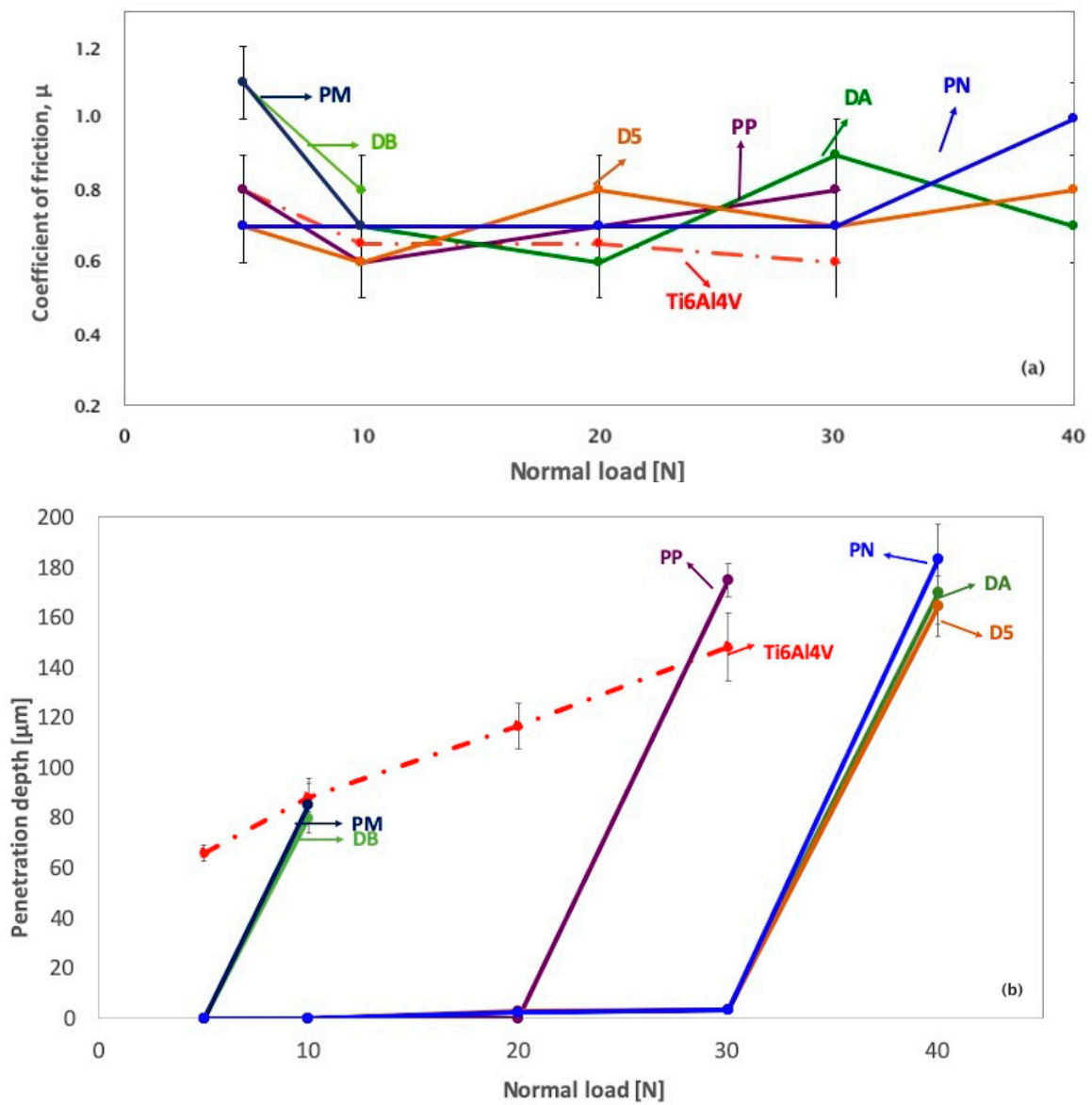
Figure 7. Average values of coefficient of friction (**a**) and maximum wear depth on blocks (**b**) as a function of normal load. In (**a**), the trend line for PM overlaps the one for DA between 5 and 10 N.
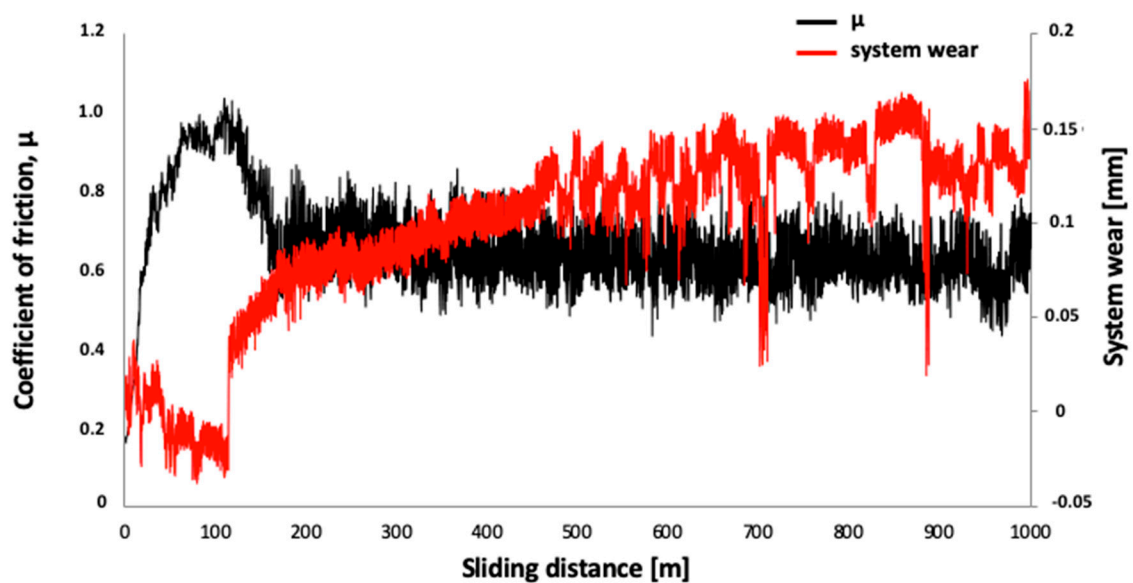
Figure 8. Friction and wear transitions for PEO layers at the critical load for coating failure: coefficient of friction (black line) and system wear (red line) as a function of sliding distance (sample DA, under a normal load of 40 N).
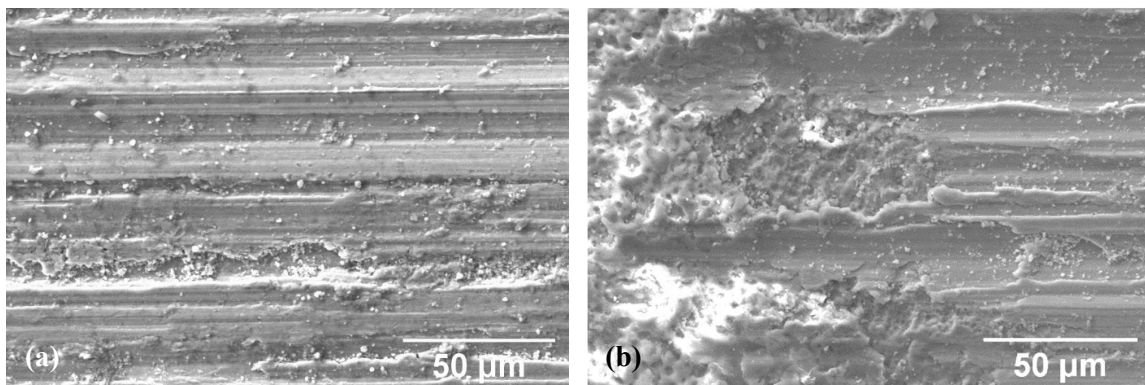

Figure 9. SEM images of wear scars on (**a**) untreated and (**b**) PEO-treated Ti-6Al-4V after the friction and wear transition that corresponds to the involvement of the substrate in the contact (i.e., coating failure).

Adhesion damage is also noticeable between the grooves, showing the same typical morphologies observed also for the untreated substrate (Figure 9a). The occurrence of these friction/wear transitions and the morphology of worn surfaces is completely comparable to the case of other PEO-treated Ti-6Al-4V samples tested in dry sliding conditions against bearing steel, discussed in a previous work by Martini et al. [25].

For this specific set of samples, the highest COF values were recorded for the as-treated (not abrasive-blasted) double layer DB (Figure 7) at 5 N. The COF of all abrasive-blasted PEO layers (with the exception of PM, discussed here below) is lower than for DB, demonstrating that the surface finishing procedure improved the frictional behaviour. Fei et al. [9] reported similar results on this phenomenon, which is due to the decrease of the abrasive component of friction, brought about by the decrease of surface roughness induced by abrasive blasting. Also, the single layer PM coating, with high roughness (Table 2) and low compactness (Figure 4), showed high COF values at 5 N. Similar to DB, also this coating failed already at 10 N, due to its detrimental combination of high roughness,

low compactness and low hardness (the latter two parameters being related, since pores and cracks negatively affect the hardness of PEO layers as shown by Curran and Clyne [37]).

For PEO layers that survived in a wider load range (namely D5 and PN), COF slightly increases on going from 30 to 40 N, due to destabilization of the iron oxide transfer layer that covers all the treated surfaces as a consequence of mild tribo-oxidation of the steel counterface. The presence of these iron oxide transfer layers, which is typically observed in the PEO-steel contact [25], is documented by the images of wear scars taken at 5 N in Figures 10 and 11 (the latter also reporting EDS and micro-Raman data).
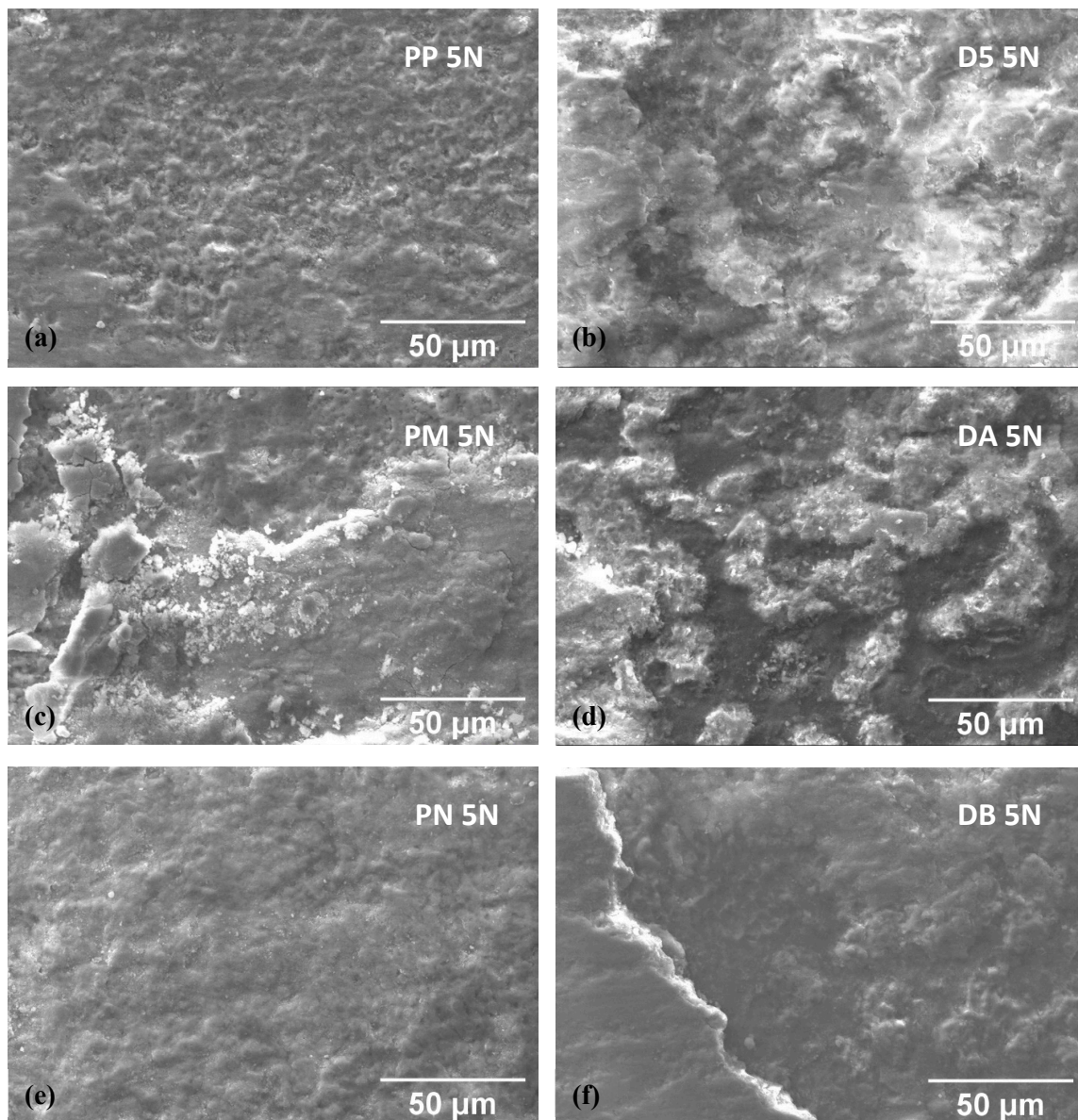

Figure 10. SEM images of wear scars at 5 N on single layers (PP: **a**, PM: **c**, PN: **e**) and double layers (D5: **b**, DA: **d**, DB: **f**) showing the presence of iron oxide based transfer layers with variable degrees of coverage and stability. Under 5 N, layers PM and DB are already at the load before coating failure and the transfer layer starts to detach.
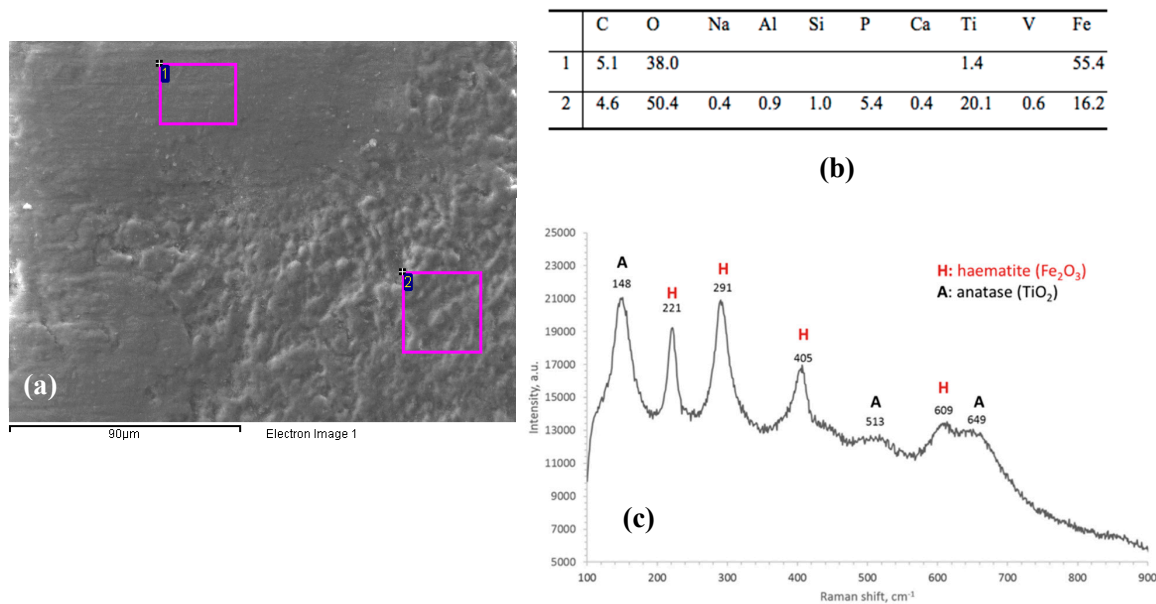
	C	O	Na	Al	Si	P	Ca	Ti	V	Fe
1	5.1	38.0						1.4		55.4
2	4.6	50.4	0.4	0.9	1.0	5.4	0.4	20.1	0.6	16.2

(b)

Figure 11. (**a**) representative SEM image of transfer layers on the surface of wear scars (single layer PN, 5 N) with (**b**) EDS data (wt.%) and (**c**) micro-Raman spectrum taken in area 1 of (**a**), showing that the thicker areas of the transfer layer mostly consist of haematite (Fe_2O_3).

These transfer layers, when formed during dry sliding against AISI 52100 at room temperature and at relatively low sliding speed (0.3 m s^{-1}), consist of haematite (Fe_2O_3) according to micro-Raman analyses (Figure 11c). Tonelli et al. [38] observed the same type of haematite-based transfer layers also for other PEO coatings in similar contact conditions.

The destabilization of the transfer layers starts to be appreciable at the load before friction and wear transition (e.g., in Figure 10c,f for layers PM and DB respectively, already being at the load before failure at 5 N and in Figure 12 for the other layers). Also, the detachment of micro-fragments from the PEO layer, which mostly occurs before complete coating failure, may contribute to increase the abrasive component of friction at high load.

As for COF, also the trend of maximum wear depth (measured on PEO-treated and untreated stationary blocks at the end of the tests) versus normal load (Figure 7b) shows the above described transitions, related to coating failure. After coating failure, in fact, wear depth of PEO-treated blocks noticeably increases with increasing normal load, achieving values comparable to the untreated substrate. However, before coating failure, all the PEO layers investigated in the present work performed better than the bare Ti-6Al-4V substrate, in terms of wear resistance.

As previously discussed for COF, the abrasive blasting process has a beneficial influence also on wear depth. By comparing the curves of samples DA and DB in Figure 7b, it is possible to notice that the removal of the porous and brittle external layer increased the critical load to failure from 10 N (DB) to 40 N (DA), probably due to a decreased tendency towards micro-crack driven damage accumulation, in the case of the smoother coating (DA).

It is worth noting that the PEO treatment in phosphate-based bath after the production of the inner layer in silicate bath (i.e., comparing S (single layer) to D5 (double layer)) was beneficial, leading to an increased critical load to failure (from 30 to 40 N). This effect can be probably ascribed to the higher compactness of D5 and hence to its increased hardness.

The critical load to failure for single layers obtained in phosphate bath increased in the following order: PM < P < PP < PN. This indicates that most layers obtained in pulsed DC perform better than the one obtained in DC (sample P) and the best tribological behaviour can be achieved for pulsed DC treatment at highest duty cycle (PN), due to combination of dense microstructure, relatively high hardness and high adhesion. In the case of PP, the unexpected good wear resistance (despite its low

adhesion and non-dense microstructure) may be due to the Si-rich top layer, formed as consequence of glass embedding during abrasive blasting (discussed in Section 3.2), which may also contribute to local enhancement of surface hardness.
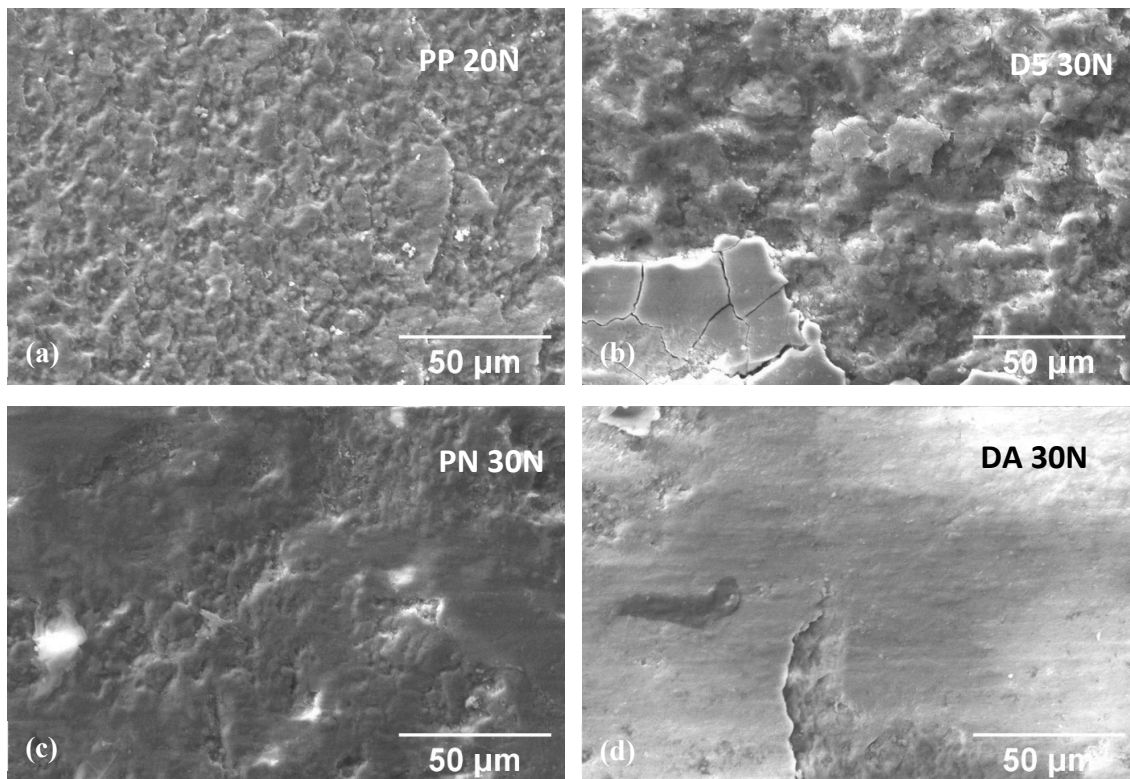

Figure 12. SEM images of wear scars at the load before coating failure for PEO coatings which survived at loads higher than 10 N: single layers (PP: **a**, PN: **c**) and double layers (D5: **b**, DA: **d**).

It is also worth noting that pulsed DC treatment at highest duty cycle (PN) attains the same critical load to failure in dry sliding as the best double layers. This is probably related to its dense microstructure and relatively high hardness. Moreover, the low roughness of PN by comparison to D5 and DA, induced by the absence of the intermediate silicate layer, is also likely to limit stress concentration at asperities, thereby limiting micro-crack driven damage, which is a typical wear mechanism associated with PEO layers as reported by Diamanti et al. [34]. The promising behaviour of PN therefore suggests that single-layer high duty cycle pulsed DC can be considered as an alternative and simpler processing route than double-layer deposition.

As regards abrasive-blasted double layers, both D5 and DA achieved the highest values of critical load to failure (40 N, Figure 7b). Their comparable performance indicates that microhardness alone is not the key parameter in influencing wear behaviour: both layers display a rather dense microstructure, hence practical adhesion plays a key role in determining the high critical load of DA, notwithstanding its lower hardness. It is also worth noting that embedding of glass residues was observed in the DA layer (as discussed in Section 3.2). As previously discussed for PP, this Si-rich surface layer may have a non-negligible beneficial influence, also predominating over other features such as microstructure, adhesion and hardness.

As for the comparison carried out under the highest normal loads (30 and 40 N) between the best-performing PEO layers (PN, D5 and DA) and reference materials (i.e., uncoated or PVD (Ti,Nb)N coated Ti-6Al-4V and CoCrMo), the average maximum wear scar depth values are reported in Figure 13.

As previously discussed, all PEO layers outperform the uncoated Ti-6Al-4V. At 30 N, all the selected PEO layers display wear depths comparable to CoCrMo (both uncoated and PVD-coated). The wear depth of PEO layers is also slightly lower than for PVD-coated Ti-6Al-4V, which is a promising

result considering that in this case the thickness of PEO layers is only slightly higher than that of the PVD coating, which is 5 μm thick). At 40 N, both the PEO the PVD layers on Ti-6Al-4V are worn out and their substrate is markedly involved in the contact. Only the PVD-coated CoCrMo still shows a very low wear depth (lower than that of the uncoated CoCrMo), due to the high load-bearing capacity of this substrate.
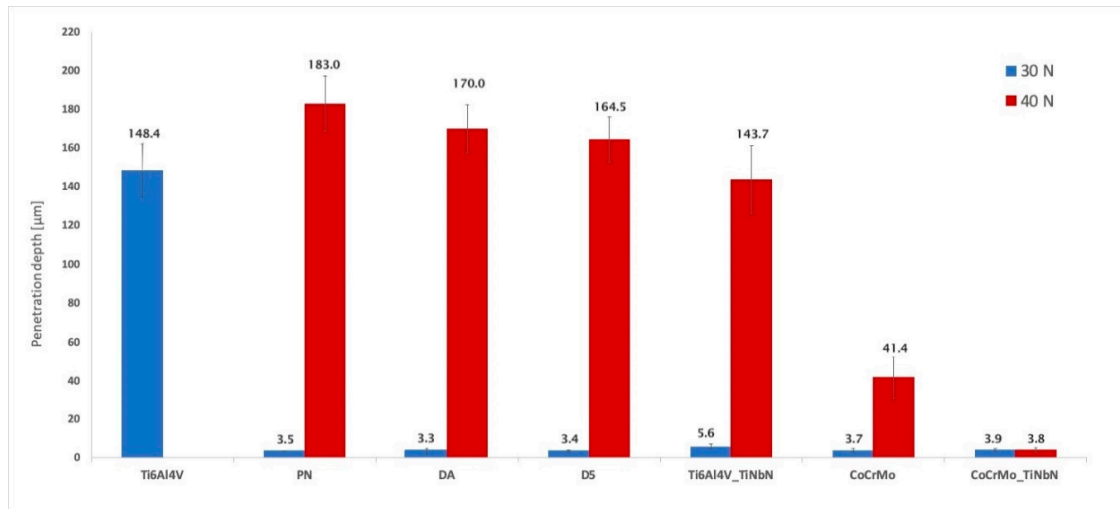

Figure 13. Wear depth values measured under normal loads of 30 and 40 N on the best-performing PEO layers and on the reference materials (uncoated or PVD (Ti,Nb)N coated Ti-6Al-4V and CoCrMo).

4. Conclusions

The dry sliding behaviour of the Ti-6Al-4V alloy, PEO-treated by using different process parameters, was assessed and correlated both to microstructure and micro-mechanical characteristics (hardness, practical adhesion). In particular, we investigated the influence on tribological behaviour of (i) layer structure (single layer, obtained in phosphate bath or double layer, obtained in silicate bath followed by phosphate bath), (ii) current mode (DC or pulsed DC), (iii) duty cycle (in case of pulsed DC deposition) and (iv) surface finishing (i.e., industrial post-treatment by abrasive blasting).

The results allowed to draw the following conclusions:

- Surface finishing by abrasive blasting with spheroidal glass beads leads to surface roughness decrease and hence to decreased friction and improved wear resistance. However, this procedure may also induce embedding of glass residues in the cortical zone of PEO layers, with an additional beneficial influence on tribological behaviour.
- The tribological behaviour of PEO layers obtained in pulsed DC tends to improve with increasing duty cycle values, due to improved microstructure and adhesion of PEO layers.
- Single-layer, high duty cycle, pulsed DC can be considered as an alternative, simpler processing route than double-layer deposition, leading to comparable wear performance.
- In the case of PEO layers obtained in the conventional DC regime, the double-layer structure (treatment in silicate bath followed by phosphate bath) beneficially affected wear behaviour.
- The best PEO layers among those developed in this study showed promising results in the comparison with reference materials. In particular, at 30 N normal load, PEO layers displayed wear depths comparable to CoCrMo (both uncoated and (Ti,Nb)N PVD-coated) and slightly lower than PVD-coated Ti-6Al-4V. At 40 N, however, both PEO layers and PVD coatings on Ti-6Al-4V underwent failure and only PVD-coated CoCrMo showed low wear depths.

Author Contributions: Conceptualization, C.M., G.R. and A.M.; methodology, C.M., G.R. and A.M.; investigation, A.G. and C.B.; data curation, C.M., A.G. and C.B.; writing—original draft preparation, A.G.; writing—review and editing, C.M., C.B., A.M. and G.R.

References

1. Chen, Q.; Thouas, G.A. Metallic implant biomaterials. *Mater. Sci. Eng. R Rep.* **2015**, *87*, 1–57. [CrossRef]
2. Jarcho, M.; Kay, J.F.; Gumaer, K.I.; Doremus, R.H.; Drobeck, H.P. Tissue, cellular and subcellular events at a bone-ceramic hydroxylapatite interface. *J. Bioeng.* **1977**, *1*, 79–92. [PubMed]
3. Huang, N.; Leng, Y.X.; Ding, P.D. Surface engineered titanium alloys for biomedical devices. In *Surface Engineering of Light Alloys*; Woodhead Publishing: Cambridge, UK, 2010; pp. 568–602.
4. Durdu, S.; Deniz, Ö.F.; Kutbay, I.; Usta, M. Characterization and formation of hydroxyapatite on Ti6Al4V coated by plasma electrolytic oxidation. *J. Alloys Compd.* **2013**, *551*, 422–429. [CrossRef]
5. Li, L.H.; Kong, Y.M.; Kim, H.W.; Kim, Y.W.; Kim, H.E.; Heo, S.J.; Koak, J.Y. Improved biological performance of Ti implants due to surface modification by micro-arc oxidation. *Biomaterials* **2004**, *25*, 2867–2875. [CrossRef] [PubMed]
6. Jiang, B.L.; Wang, Y.M. 5-Plasma electrolytic oxidation treatment of aluminium and titanium alloys. In *Surface Engineering of Light Alloys: Aluminium, Magnesium and Titanium Alloys*; Dong, H., Ed.; Woodhead publishing Limited: Cambridge, UK, 2010; pp. 110–146. ISBN 1845699459.
7. Shrestha, S.; Dunn, B.D. Plasma electrolytic oxidation and anodising of aluminium alloys for spacecraft applications. In *Surface Engineering of Light Alloys*; Woodhead Publishing: Cambridge, UK, 2010; pp. 603–641.
8. Chen, Y.; Cheng, T.; Nie, X. Wear failure behaviour of titanium-based oxide coatings on a titanium alloy under impact and sliding forces. *J. Alloys Compd.* **2013**, *578*, 336–344. [CrossRef]
9. Chen, F.; Zhou, H.; Chen, C.; Xia, Y.J. Study on the tribological performance of ceramic coatings on titanium alloy surfaces obtained through microarc oxidation. *Prog. Org. Coat.* **2009**, *64*, 264–267.
10. Wang, Y.M.; Jiang, B.L.; Guo, L.X.; Lei, T.Q. Tribological behavior of microarc oxidation coatings formed on titanium alloys against steel in dry and solid lubrication sliding. *Appl. Surf. Sci.* **2006**, *252*, 2989–2998. [CrossRef]
11. International Standard ISO 20502. *Fine Ceramics (Advanced Ceramics, Advanced Technical Ceramics)—Determination of Adhesion of Ceramic Coatings by Scratch Testing*, 1st ed.; Korean Agency for Technology and Standards: Chungcheongbuk-do, Korea, 2002; Volume 6, pp. 1–16.
12. ASTM Standard G77. *Standard Test Method for Ranking Resistance of Materials to Sliding Wear Using Block-on-Ring Test*; ASTM International: West Conshohocken, PA, USA, 2017.
13. Ceschini, L.; Chiavari, C.; Marconi, A.; Martini, C. Influence of the countermaterial on the dry sliding friction and wear behaviour of low temperature carburized AISI316L steel. *Tribol. Int.* **2013**, *67*, 36–43. [CrossRef]
14. Borgese, L.; Gelfi, M.; Bontempi, E.; Goudeau, P.; Geandier, G.; Thiaudière, D.; Depero, L.E. Young modulus and Poisson ratio measurements of TiO_2 thin films deposited with Atomic Layer Deposition. *Surf. Coat. Technol.* **2012**, *206*, 2459–2463. [CrossRef]
15. Soares, P.; Mikowski, A.; Lepienski, C.M.; Santos, E.; Soares, G.A.; Filho, V.S.; Kuromoto, N.K. Hardness and elastic modulus of TiO_2 anodic films measured by instrumented indentation. *J. Biomed. Mater. Res. Part B Appl. Biomater.* **2008**, *84*, 524–530. [CrossRef]
16. Galetz, M.C.; Seiferth, S.H.; Theile, B.; Glatzel, U. Potential for adhesive wear in friction couples of UHMWPE running against oxidized zirconium, titanium nitride coatings, and cobalt-chromium alloys. *J. Biomed. Mater. Res. Part B Appl. Biomater.* **2010**, *93*, 468–475. [CrossRef]
17. Malchesky, P.S. Artificial Organs 2003: A Year in Review. *Artif. Organs* **2004**, *28*, 410–424. [CrossRef]
18. Paschoal, A.L.; Vanâncio, E.C.; Canale, L.C.F.; Silva, O.L.; Huerta-Vilca, D.; Motheo, A.J. Metallic Biomaterials TiN-Coated: Corrosion Analysis and Biocompatibility. *Artif. Organs* **2003**, *27*, 461–464. [CrossRef]
19. *Standard Specification for Wrought Cobalt-28Chronium-6Molybdenum Alloys for Surgical Implants (UNS R31537, UNS R31538, and UNS R31539)*; ASTM F1537; ASTM International: West Conshohocken, PA, USA, 2011.

20. *Standard Test Methods for Determining Average Grain Size*; ASTM E112; ASTM International: West Conshohocken, PA, USA, 2012.

21. Bouchard, M.; Smith, D.C. *Raman Spectroscopy in Archaeology and Art History*; Edwards, H.G.M., Chalmers, J.M., Eds.; Royal Society of Chemistry: London, UK, 2005; pp. 429–464. ISBN 9780854045228.

22. Friedemann, A.E.R.; Thiel, K.; Haßlinger, U.; Ritter, M.; Gesing, T.M.; Plagemann, P. Investigations into the structure of PEO-layers for understanding of layer formation. *Appl. Surf. Sci.* **2018**, *443*, 467–474. [CrossRef]

23. Xue, W.; Deng, Z.; Lai, Y.; Chen, R. Analysis of Phase Distribution for Ceramic Coatings Formed by Microarc Oxidation on Aluminum Alloy. *J. Am. Ceram. Soc.* **1998**, *81*, 1365–1368. [CrossRef]

24. Khan, R.H.U.; Yerokhin, A.L.; Li, X.; Dong, H.; Matthews, A. Influence of current density and electrolyte concentration on DC PEO titania coatings. *Surf. Eng.* **2014**, *30*, 102–108. [CrossRef]

25. Martini, C.; Ceschini, L.; Tarterini, F.; Paillard, J.M.; Curran, J.A. PEO layers obtained from mixed aluminate–phosphate baths on Ti–6Al–4V: Dry sliding behaviour and influence of a PTFE topcoat. *Wear* **2010**, *269*, 747–756. [CrossRef]

26. Wang, Y.; Lei, T.; Jiang, B.; Guo, L. Growth, microstructure and mechanical properties of microarc oxidation coatings on titanium alloy in phosphate-containing solution. *Appl. Surf. Sci.* **2004**, *233*, 258–267. [CrossRef]

27. Yerokhin, A.L.; Nie, X.; Leyland, A.; Matthews, A. Characterisation of oxide films produced by plasma electrolytic oxidation of a Ti–6Al–4V alloy. *Surf. Coat. Technol.* **2000**, *130*, 195–206. [CrossRef]

28. Wang, Y.M.; Jiang, B.L.; Lei, T.Q.; Guo, L.X. Microarc oxidation coatings formed on Ti6Al4V in Na2SiO3 system solution: Microstructure, mechanical and tribological properties. *Surf. Coat. Technol.* **2006**, *201*, 82–89. [CrossRef]

29. Yeung, W.K.; Reilly, G.C.; Matthews, A.; Yerokhin, A. In vitro biological response of plasma electrolytically oxidized and plasma-sprayed hydroxyapatite coatings on Ti–6Al–4V alloy. *J. Biomed. Mater. Res. B Appl. Biomater.* **2013**, *101*, 939–949. [CrossRef]

30. Mohammadi, H.; Hafezi, M.; Nezafati, N.; Heasarki, S.; Nadernezhad, A.; Ghazanfari, S.M.H.; Sepantafar, M. Bioinorganics in Bioactive Calcium Silicate Ceramics for Bone Tissue Repair: Bioactivity and Biological Properties. *J. Ceram. Sci. Technol.* **2014**, *5*, 1–12.

31. Aliasghari, S.; Němcová, A.; Skeldon, P.; Thompson, G.E. Influence of coating morphology on adhesive bonding of titanium pre-treated by plasma electrolytic oxidation. *Surf. Coat. Technol.* **2016**, *289*, 101–109. [CrossRef]

32. Dehnavi, V.; Luan, B.L.; Liu, X.Y.; Shoesmith, D.W.; Rohani, S. Correlation between plasma electrolytic oxidation treatment stages and coating microstructure on aluminum under unipolar pulsed DC mode. *Surf. Coat. Technol.* **2015**, *269*, 91–99. [CrossRef]

33. Galvis, O.A.; Quintero, D.; Castaño, J.G.; Liu, H.; Thompson, G.E.; Skeldon, P.; Echeverría, F. Formation of grooved and porous coatings on titanium by plasma electrolytic oxidation in H2SO4/H3PO4 electrolytes and effects of coating morphology on adhesive bonding. *Surf. Coat. Technol.* **2015**, *269*, 238–249. [CrossRef]

34. Diamanti, M.V.; Sebastiani, M.; Mangione, V.; Del Curto, B.; Pedeferri, M.P.; Bemporad, E.; Cigada, A.; Carassiti, F. Multi-step anodizing on Ti6Al4V components to improve tribomechanical performances. *Surf. Coat. Technol.* **2013**, *227*, 19–27. [CrossRef]

35. Tekin, K.C.; Malayoglu, U.; Shrestha, S. Tribological behaviour of plasma electrolytic oxide coatings on Ti6Al4V and cp-Ti alloys. *Surf. Eng.* **2016**, *32*, 435–442. [CrossRef]

36. Durdu, S.; Usta, M. The tribological properties of bioceramic coatings produced on Ti6Al4V alloy by plasma electrolytic oxidation. *Ceram. Int.* **2014**, *40*, 3627–3635. [CrossRef]

37. Curran, J.A.; Clyne, T.W. Porosity in plasma electrolytic oxide coatings. *Acta Mater.* **2006**, *54*, 1985–1993. [CrossRef]

38. Tonelli, L.; Pezzato, L.; Dolcet, P.; Dabalà, M.; Martini, C. Effects of graphite nano-particle additions on dry sliding behaviour of plasma-electrolytic-oxidation-treated EV31A magnesium alloy against steel in air. *Wear* **2018**, *404*, 122–132. [CrossRef]